ADVANCED THEORY AND SIMULATIONS
www.advtheorysimul.com

Self Assembly of Patchy Anisotropic Particle Forming Free Standing Monolayer Film

*Vikki Anand Varma, Kritika, Jaskaran Singh, and Sujin B. Babu**

Synthesizing thin films using self assembly is one of the important challenges which needs to be addressed for making engineered material using colloidal particle, necessary for creating novel material for photonic, filtration application, etc. Here, a simple model of prolate ellipsoidal particle with two directional bonds is presented and the phase behavior is studied using NVT and NpT Monte Carlo simulation. It is observed that for anisotropic particles with patches two different type of 3D ordered structures are formed along with thermodynamically stable monolayer which is confirmed using thermodynamic integration. The phase diagram shows that the desired 2D super structure can be created using simple self assembly route.

1. Introduction

There has been significant development in the field of template based engineered materials in colloids.[1–3] The desired super structures of colloids can be formed by using anisotropic particles,[4] manipulating the interaction between colloidal particles functionalized with DNA[5] or introducing directional bonds between colloidal particles.[6,7] Various applications have been proposed for the colloidal thin film like materials with unique photonic[3] or plasmonic sensing[8] properties. For the formation of thin films a substrate[4,9] is required, and the drawback of the method being the rupture of mechanically sensitive thin film from the wafer. The free standing film[10,11] formed by the self-assembling process can overcome this drawback as it does not require the support of the substrate to grow, although scaling up the structures is very challenging.

To engineer materials with specific properties through self-assembly the patchy colloidal particle are considered as ideal building blocks.[12,13] Patchy particle usually have a hard core component with decorated patches on the surface.[12,14] The hard core component can have be symmetric shape like the sphere[12] or asymmetric shape like ellipsoids,[15] rods,[16] 2D structure,[17] etc. Most of the studies have concentrated on spherical patchy particles. They exhibit rich phase properties which include crystals, bundles, chains, etc.[6,7,18–24] Only a few studies have concentrated on anisotropic hard-core, for example, spheroids.[25–27]

In the present work we have performed Monte-Carlo simulation in both NpT as well as NVT ensemble. For the NVT simulation we have used Brownian cluster dynamics (BCD).[28–32] BCD was originally developed to study both reversible[33,34] and irreversible[35–39] aggregation of spherical particles with square well interaction. The bundle formation of lysozyme protein was mimicked after incorporation of patchy interaction with the isotropic potential[31,40–42] for spherical particles using BCD. Later the BCD was extended to simulate the structure and dynamics for both prolate and oblate particles.[32] In the present study we have focused on prolate particle with two-patches placed at the opposite ends of the major axis. Here, we control the valency by controlling the patch angle as we have kept the patch width a constant. Thermodynamic calculation showed that through the self assembly of ellipsoidal patchy, the crystals and fluids are the stable structure along with the free-standing ordered monolayer structure.

The paper is arranged the following way, in Section 2, we have explained the Kern–Frenkel potential applied to anisotropic particles. We have also explained the Brownian cluster dynamic method used to simulate the NVT ensemble, followed by NpT ensemble calculation using Monte-Carlo method. In the Section 3 we have shown that the ellipsoidal particles with patches at finite temperature and pressure undergo a gas crystal phase transition. The crystal formed has HCP structure. We have identified two types of HCP crystal structures based on the number of bonds by the system. Surprisingly we were also able to identify a small range of temperature and pressure, were a free standing monolayer of thin film was the thermodynamically stable structure. This results were verified using both floppy box simulation as well as free energy calculation. We have also performed thermodynamic integration and have plotted the phase diagram for the system. We have proposed that the self assembly can be used to produce free standing film, which is followed by conclusion in Section 4

2. Simulation Method

We have used discontinuous potential as an approximation of molecular potential. The shape of the prolate hard core potential is defined by the aspect ratio $p = a/b$, where, a and b are the length of the semi-major and semi-minor axis, respectively. In the

V. A. Varma, Kritika, J. Singh, S. B. Babu
Out of Equilibrium Group
Department of Physics
Indian Institute of Technology Delhi
New Delhi 110016, India
E-mail: sujin@physics.iitd.ac.in

The ORCID identification number(s) for the author(s) of this article can be found under https://doi.org/10.1002/adts.202200666

DOI: 10.1002/adts.202200666

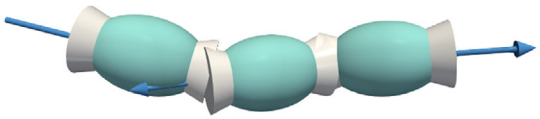

Figure 1. Three bonded ellipsoidal particles are shown. The arrows represent the orientation vectors ($\hat{n}$) and the white conic section represents the patches.

present study we have kept $p = 1.5$ so that we can avoid nematic transition in these systems. We represent an ellipsoid of revolution (ER) with a unit vector $\hat{n}$ (also called director), along the symmetry axis and the center of mass position vector as shown by the arrows in **Figure 1**. ER volume is kept at $\pi/6$, which is equal to the volume of a sphere of unit diameter $d = 1$. To simulate the particles with highly directional bonding properties, the hard ellipsoidal particle is superimposed with conical patches as shown in Figure 1. The pair potential between particle i,j with director $\hat{n}_i$, $\hat{n}_j$ and inter-particle distance $\mathbf{r}_{ij}$ is defined as

$$U_{i,j} = \begin{cases} -u_\circ \cdot \sigma_{i,j}(\mathbf{r}_{i,j}, \hat{n}_i, \hat{n}_j) \cdot \chi_{i,j}(\hat{r}_{i,j}, \hat{n}_i, \hat{n}_j) \\ \infty \qquad \text{Hardcore} \qquad \text{overlap} \end{cases} \tag{1}$$

where u_o is the depth of the square well potential with the interaction range $\varepsilon = 0.1$. We define $h_{i,j}(\mathbf{r}_{i,j}, \hat{n}_i, \hat{n}_j)$ as the distance between the surfaces of the hard cores, calculated by using ellipsoids contact function (ECF).[32] $\boldsymbol{\sigma}_{\mathbf{i,j}}$ and $\boldsymbol{\chi}_{\mathbf{i,j}}$ is defined as

$$\sigma_{i,j} = \begin{cases} 1 & h_{i,j} < \varepsilon \\ 0 & \text{Otherwise} \end{cases} \tag{2}$$

$$\chi_{i,j} = \begin{cases} 1 & |\hat{r}_{ij}.\hat{n}_i| \geq \cos(\omega), |\hat{r}_{ji}.\hat{n}_j| \geq \cos(\omega) \\ 0 & \text{Otherwise} \end{cases} \tag{3}$$

The patches are located on the opposite end of the major axis and ω is the patch angle. In the present work we are not restricting the number of bonds per patch but observed that by tuning ω and p the maximum number of bonds formed per patch can be controlled.

2.1. Brownian Cluster Dynamics

BCD is an NVT Monte-Carlo simulation technique, which also reproduce the dynamics and kinetics of molecular dynamics (MD) simulations for square-well potential.[31] BCD consist of two steps first is the cluster construction step and the second is the movement step. In the cluster construction step when two patchy ellipsoidal particles are within each other's interaction range, a bond is formed with probability α. If a bond already exists then they are broken with probability β. Thus the probability for a bond to exist is given $P = \alpha/(\alpha + \beta)$, such that the potential is given by $u = \ln(1 - P)$. The bond formation and disassociation leads to formation of clusters which is identified as the collection of ellipsoidal particle bonded through the patches. For the sake of calculation a monomer is considered as a cluster of size 1. The movement step of the ellipsoidal particles comprises of both translation and rotational motion. In the movement step the center of mass of every ellipsoidal particle is translated with a small step size s_t. For t_{sim} movement step the center mass undergoes a random walk such that the mean squared displacement is given by $t_{\text{sim}}s_t^2$. As we make the step size very small the center of mass undergoes a Brownian motion with physical time given by $t_0 = t_{\text{sim}}s_t^2$. Thus unit of time t_0 is defined as the time taken by the center of mass of an ellipsoids to travel a unit distance.[32] The orientation of the symmetry axis of the ellipsoid undergoes a random walk on a 2D plane with a step size s_r in a random direction which mimic rational motion as shown by Varma et al.[32] If either of the movement steps leads to the hard core to overlap with other ellipsoidal particles or break an already formed bond then that movement step of that particular ellipsoid is rejected. We have already shown that if the step size is smaller than $0.005d$, the diffusion coefficient of the ellipsoidal particle obtained from BCD agrees with the analytical calculation of Perrin et al.[32]

2.2. NPT Simulation in a Floppy Box

To accurately calculate the phase diagram we have also performed Monte-Carlo NPT simulation. A random distribution of the ellipsoidal particles is taken in a cubic box[43,44] as the initial configuration. For this configuration a particle is randomly selected and an attempt is made to move the center of mass with a step length $\pm\delta s$, which is randomly selected from the range $0.1d - 0.005d$. Similar to the NVT simulation we also perform rotational movement using a quaternion over $\hat{n}$, by an angle $\pm\delta\theta$, which is randomly selected within the range 0.02–0.01. After the movement step an attempt is made to change the volume and shape of the box by randomly selecting one of the edges of the simulation box and changing its edge vector with some random displacement by $\pm\delta r$, within range $\pm 0.5 - \pm 0.005$. The new configuration is accepted using metropolis Monte-Carlo method. We make sure that the acceptance ratio is always between 30% and 40%. When the acceptance ratio falls below 30%, we reduce the length of the step size by a factor 0.95. In the case the acceptance ratio increase beyond 40% we increase the step length through the factor 0.95 as well. To avoid any unphysical shape of the simulation box, we use the lattice reduction technique[45] as well as restrict the angles between edges in the range 30–150°.[46] Simulation starts at a fixed temperature, while varying pressure from low to high, up to the desired value.

3. Results

3.1. Structural Properties

To predict equilibrium structures at various temperature and pressure, we performed floppy box simulation[47] with very few number of particles in the range of 2 to 8 as shown in **Figure 2**. In this method, shape and volume of the box changes at a particular pressure and temperature. We initialize the system with random positional and orientation distribution of the spheroids within a cubic box. At constant temperature the pressure is varied from lower to higher values till the desired pressured is reached. For the equilibriation of the ellipsoidal particle we perform random translation and rotation of the ellipse for 10^6–10^7 steps until the number of bonded neighbors per particle remained constant.

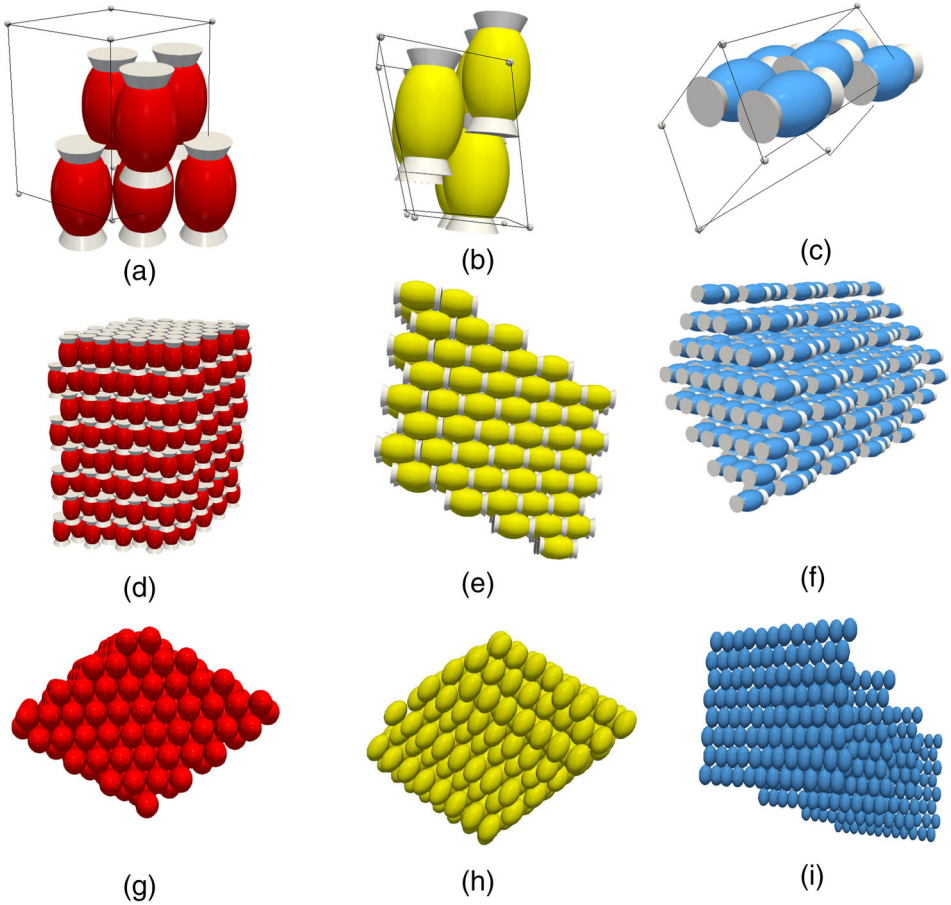

Figure 2. Unit cell (top row) of different crystal structures as predicted by the floppy simulation and corresponding bulk system (bottom row), with $p = 1.5$ and $\cos(\omega) = 0.9$ a) Type I crystal, b) Type II crystal, and c) monolayer. d) The Type-I crystal, at $k_B T/u_o = 0.15$ and $p\sigma^3/k_B T = 0.5$. e) Type-II crystal at $k_B T/u_o = 0.2$ and $p\sigma^3/k_B T = 10$. f) The monolayer at $k_B T/u_o = 0.2$ and $p\sigma^3/k_B T = 6$. The corresponding top view of crystal are shown g) Type I, h) Type II, and i) monolayer. Patches have been shown with white color cone.

The structures thus formed are replicated in a larger box with particle number in between 600–1000 and the system is then again equilibrated. To identify different structures formed inside the box we follow the criteria as proposed by Vissers et al.[48] Structure with the same number of nearest neighbors are considered identical, if the difference in the respective densities of structures are less than 0.05 as well as the difference between the pair correlation and orientational correlation function is between 0.9 and 1. With this criterion, three stable structures (Figure 2) were identified for the relevant range of temperature and pressure.

The unit cell as obtained from the floppy box simulation for Type I (Figure 2a), Type II (Figure 2b), and monolayer (Figure 2c) are shown. The structures formed with a few number of particles are replicated to form bulk crystal which is further equilibriated using floppy box simulation. The structure thus formed are shown in Figure 2d for Type I crystal, Figure 2e for Type II crystal, and Figure 2e for free standing monolayer. In type-I crystal each particle is bonded with its six nearest neighbors and the patch vector is always perpendicular to the plan of stacking. Thus the bonds are formed with ellipsoidal particles along the layers as well as with adjacent layers of ellipsoid as can be observed in Figure 2g. In Type II crystal, particles are bonded only within the layer, with a maximum of four bonded nearest neighbors and the patch vector can be observed aligned along a single layer of stacking see Figure 2h. The layers are arranged in a periodic manner and interaction between layer are only through the hard core repulsion see **Figure 3**b. In Type II crystal we observe that the adjacent layer are shifted in the direction perpendicular to the patch vector compared to Type I crystal. At moderate temperature and relatively smaller volume fraction (low pressure), the periodic stacking of the Type-II crystal breaks, leading to the random orientation of the layers. This leads to the formation of stable configuration of monolayer free standing films, as shown in the Figure 2f as well as clearly observed in the Figure 2i (top view). These structures were further simulated using the NVT ensemble starting from a random distribution of ellipsoidal particle with periodic boundary condition. Depending on ϕ and the interaction strength we obtained the same structure as observed in floppy box simulation. Type-I crystals (Figure 3a) are formed when energy is favored over entropy, which happens at low temperatures regime. Coexistence of the free standing monolayer film with the gas particles can be observed (see Video S1,

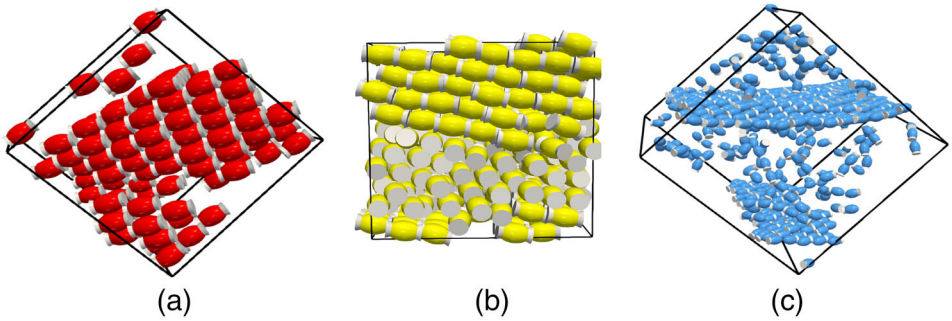

Figure 3. The structures predicted by floppy simulation, obtained in the NVT simulation for the system with $p = 1.5$ and $\cos(\omega) = 0.9$. From left to right. a) Red corresponds to the Type-I crystal, at $k_B T/u_o = 0.15$ and $\phi = 0.55$. b) Yellow: Type-II crystal at $k_B T/u_o = 0.20$ and $\phi = 0.55$. While c) blue is the monolayer at $k_B T/u_o = 0.114$ and $\phi = 0.06$. Patches have been shown with white color cone, along the $\hat{n}$ of spheroids.

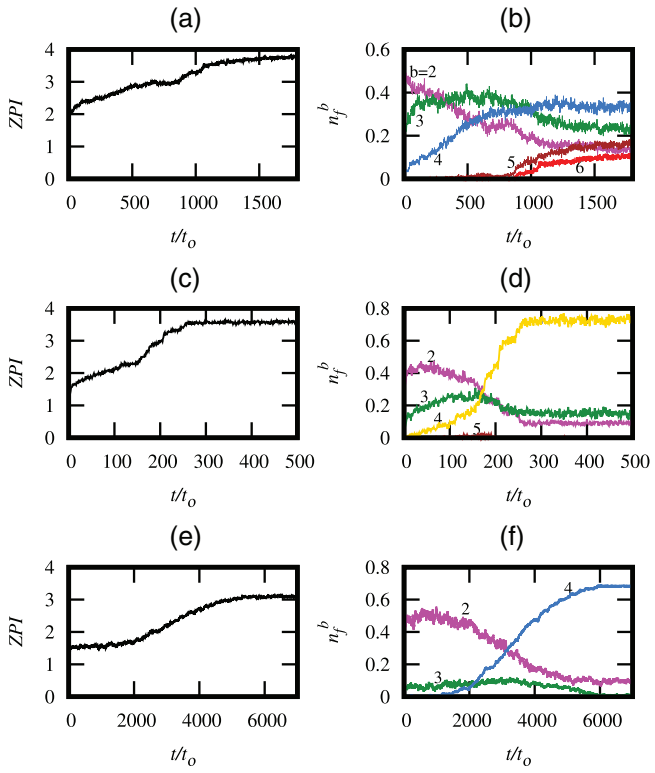

Figure 4. Average bonded nearest neighbor; ZPI shown as a function of time on the left and the particle fraction with the given number of bonded neighbors, as indicated in the figure is shown on the right. a,b) Type-I crystal at $k_B T/u_o = 0.15$ and $\phi = 0.55$. c,d) Type-II crystal at $k_B T/u_o = 0.20$ and $\phi = 0.55$. e,f) Monolayer at $k_B T/u_o = 0.114$ and $\phi = 0.06$.

Supporting Information) for a system equilibriated in NVT ensemble (Figure 3c) at $\phi = 0.06$ and $k_B T/u_\circ = 0.114$, as expected from the floppy box simulation(Figure 2b).

The change in the number of bonded neighbors can be observed in the constant NVT simulation. In **Figure 4**a we have shown the evolution of the average number of bonded neighbors ZPI for $\phi = 0.55$ at $u_\circ/k_B T = 0.114$. As the system start to aggregate from a random ellipsoidal distribution the ZPI increases over time until it reaches a steady state which in the present case is <4. In Figure 4b we have shown the evolution of the fraction of particles bonded to a particular ellipsoid n_f^b as a function of time, such that $b = 2$ means 2 particles are bonded to an ellipsoidal particle. We can observe that n_f^b for $b = 2$ and 3 are maximum at initial times, then the fraction of $b = 4$ number of bonds increases indicating the formation of an ordered structure. After a time of $t/t_0 > 1000$ we observe particles having five and six bonds increases leading to the formation of bulk crystal. In Figure 4c at $K_B T/u_\circ = 0.2$ and $\phi = 0.55$ we observe the formation of Type-II crystal, the average number of bonded neighbors is below 4 as Type-I crystal. The evolution of the fraction of particles having two and three bonds decreases with time and the fraction of particles having four bonds increases with time similar to Type I crystal. We also observe for longer times the fraction of particles having five and six bonds are absent (Figure 4d) for these crystal essentially differentiating Type I from Type II crystal. In Figure 4e we have shown the evolution of ZPI as a function of time for the case where the monolayer is formed. Here, we also observe that the n_f^4 increases and stagnates while n_f^3 and n_f^2 decrease with time similar to the Type II crystal.

In **Figure 5** we have shown the pair correlation function $G(r)$ as obtained from the floppy box simulation, which is compared with the structure obtained from the NVT simulation. The $G(r)$ obtained from the floppy box simulation shows a sharp peak as there is no presence of gas particles, whereas from the NVT simulation we obtained broad peaks. The peaks of the Type-I crystal as obtained from floppy box simulation and NVT simulation almost agrees with each other, confirming that we have reached near equilibrium state as shown in Figure 5a. In an NVT simulation the crystal coexist with the gas particle, whereas in floppy box simulation only the equilibrium crystal will be present. Thus when we calculate the $G(r)$ of these system in a NVT ensemble we observe a shift in the position of peaks due to the presence of gas particles. The Type II crystals are structurally different from the Type I crystals as we can observe more peaks in $G(r)$ see Figure 5. The reason is observed from floppy box simulation see in Figure 1b, as there is a slight shift in the particle position between adjacent layers for Type-II crystals. All the peaks in $G(r)$ of the monolayer can be observed both in Type I and Type II crystals, indicating that the arrangement of a single layer is the same in both the crystal types see Figure 5c.

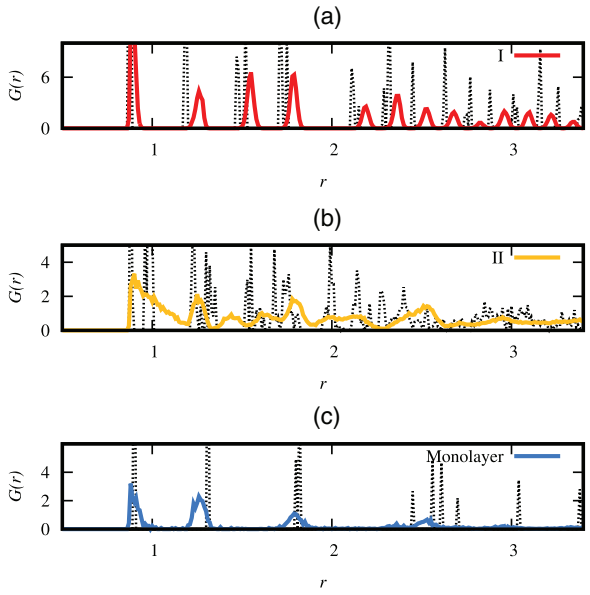

Figure 5. Pair correlation function $G(r)$ corresponding to the NVT ensemble (solid line) is compared with the structure predicted by the floppy simulation (dotted line). a) Type I crystal at $k_BT/u_o = 0.15$ and $\phi = 0.55$ b) Type-II crystal at $k_BT/u_o = 0.20$ and $\phi = 0.55$. c) Monolayer at $k_BT/u_o = 0.20$ and $\phi = 0.55$.

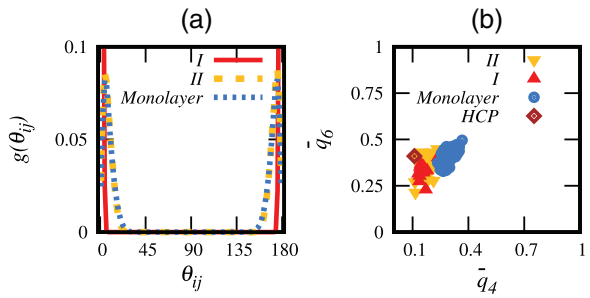

Figure 6. $\overline{q_6}$ and $\overline{q_4}$ have been shown for different structures, indicating the presence of ordered phases obtained in NVT ensembles.

For the spherical particle of the two patches, it has already been shown that they form the Kagome lattice.[49] For the prolate ellipsoidal particle we have calculated the distribution $g(\mathbf{n}_i \cdot \mathbf{n}_j)$, where $\mathbf{n}_i$ is the unit vector along the patch for the ith particle. In **Figure 6**a we can observe that in all the three types of crystal we observe only two peaks at ≈0 and ≈ π, which means that all patch vectors are parallel or antiparallel to each other. We can also observe that the width of the distribution is wider for Type-II and monolayer structure because they have more freedom to move within the bonds as the maximum number of neighbors is ≤4, compared to Type-I crystal which is ≤6. To distinguish between different crystal structures, we calculated $\overline{q_6}$ and $\overline{q_4}$, as shown in Figure 6b. We observe that all the ordered structures are closer to the HCP crystal value. We believe as limited number of directional bonds are formed due to the finite patch width and patch angle the system prefers HCP arrangement at finite temperature.

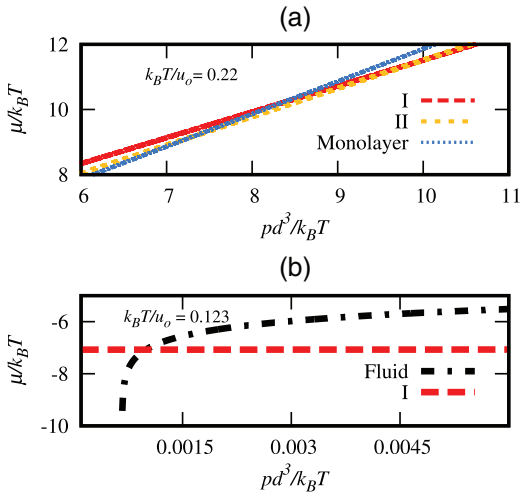

Figure 7. p–μ curve shown for different phases at $k_BT/u_o = 0.22$. p have been expressed in the unit of k_BT/d^3, while μ in the unit of k_BT. a) The intersection point of the two lines shows the coexistence of Type I crystal and fluid. b) The intersecting line show the phase coexistence of Type I, Type II, and monolayer crystals.

3.2. Phase Diagram

To draw the phase diagram we calculated chemical potential of the crystal from the free energy calculation using Einstein crystal method[47,50–52] see Supporting Information. A co-existence point of two states is identified when the chemical potential of both the crystal structure are the same in either constant pressure or constant temperature as shown in **Figure 7**a. At $K_BT/u_o = 0.22$ we can observe that as the pressure is increased the chemical potential also increases for the crystal structures. For $pd^3/k_BT \approx 7.2$ we observe that μ/k_BT of both monolayer crystal and Type II crystal intersect which is a coexistence point. $pd^3/k_BT < 7.2$ we observe that monolayer has a minimum chemical potential, thus making it the most stable structure. At $pd^3/k_BT \approx 10$ we observe that μ/k_BT of both Type I and Type II cross over each other giving us another coexistence point. We also observe that $7.2 < pd^3/k_BT < 10$ crystal Type I have the minimum chemical potential thus making it the most stable structure at these pressure and temperature. When $pd^3/k_BT > 10$ Type I is the stable structure as it has the minimum chemical potential of all the three crystal. In order to calculate the phase diagram through thermodynamic integration,[53] the free energy of the fluid was calculated using NVT and semi-grand canonical simulation[54,55] see Supporting Information. We calculated the chemical potential μ/k_BT[56] from the free energy calculation shown in Figure 7b for $k_BT/u_o = 0.123$. The point of intersection of the fluid curve and the crystal Type-I is identified as a coexistence point on the phase diagram.

Figure 8a shows the phase diagram in the T–p plane calculated by integrating the Clausius–Clapeyron equation using the Kofke method[48,57,58] see Supporting Information. At low pressure and temperature regime, we can observe the coexistence line between the Type I crystal and the fluid. Here, we would like to mention, we always observed the formation of a metastable monolayer, when simulated from a random ellipsoidal

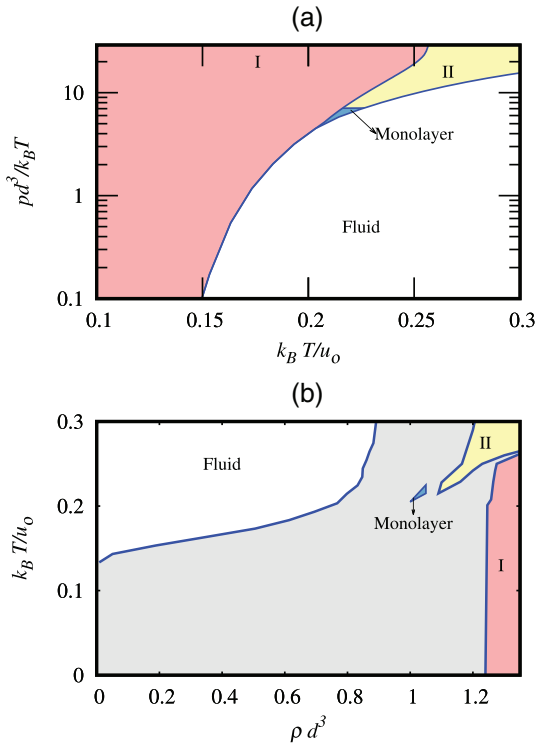

Figure 8. a) p–T phase-diagram exhibiting the location of various phases have been shown for the system of spheroids with $p = 1.5$ and $\cos(\omega) = 0.9$. p have been expressed in the unit of k_BT/d^3, while k_BT in the unit of u_o. Blue solid line represents the coexistence point among the various phases. b) ρ–T phase-diagram showing the location of various phases for the system of spheroids with $p = 1.5$ and $\cos(\omega) = 0.9$. ρ have been expressed in the unit of $1/d^3$. Blue solid line represents the coexistence point.

configuration. In the presence of a seed of Type I, we observed that the growth of the monolayer was suppressed and the Type I crystal started to grow. Thus Type-I crystal was the most stable configuration confirmed through our chemical potential calculation in this range. Pressure along the coexistence line of Type-I/fluid increases monotonically with increasing temperature. At temperature $k_BT/u_o \approx 0.23$, the fluid co-exists with the monolayer. As we further increase the temperature, the coexistence pressure increases further and finally leads the random stacking of monolayer which ultimately forms Type-II crystal. The co-existence line between Type I/Type II becomes nearly parallel to the pressure axis, for the high temperature region, indicating that for very high temperature $k_BT/u_o \geq 0.28$ and $pd^3/k_BT \geq 0.35$ only fluid and Type II can co-exist.

In Figure 8b we have shown the ϕ–T phase diagram calculated using thermodynamic integration. At low temperatures and volume fractions, we observe the coexistence of the fluid phase and the Type-I crystal. The monolayer, although confined to a very small region in the phase diagram of T and ρ is a stable configuration. Increasing the temperature from ≈0.22 leads the fluid to coexist with Type-I, monolayer and Type-II, which we have also confirmed using the chemical potential calculation as well. Upon further increase in temperature, a coexistence between fluid and Type-II can only be observed. As the density increases we observe that the forbidden region between Type-I and Type-II narrows down as well. We would also like to mention that in the present study we did not observe a metastable liquid-gas transition.

4. Discussion and Conclusion

Liu et al.[8] have shown experimentally that by varying the patch angle between 55–97° of the prolate particle they obtained 2D and quasi-2D structures. We have shown for one particular patch angle that thermodynamically stable monolayer free standing film can be formed. As shown experimentally the long range ordered 2D[8] structure was seen only for small patch angles consistent with the present work. It was shown that using metal–organic framework and depletion interaction induced by ionic amphiphiles a variety of colloidal superstructures were created which included 1D chains, crystalline 2D films and quasi 3D supercrystals on a surface. They changed the shape of the anisotropic particle to get the desired structure. In the present work we have kept the shape of the particle and the interaction range the same, while changing the thermodynamics of the systems, obtaining free standing monolayer 2D films and 3D super crystal structures without the help of interfaces.

In the present work we have simulated the aggregation of prolate particles with two patches that interact via the Kern–Frenkel potential. The aspect ratio of the particles is 1.5, and thus the system will never undergo a nematic transition. The stability of the crystalline structure was established using the floppy box simulation method, where we observed two type of crystal structures. Type I crystal had particles with valency >4, while Type II crystal have particles with atmost valency 3. Surprisingly we also observed the presence of thermodynamically stable monolayer of free standing thin film as well. The phase diagram of the system was obtained by using thermodynamic integration which also confirmed the existence of the monolayer of colloids. The calculation of bond orientation parameter showed that the crystal are closer to HCP arrangement. The phase diagram was calculated by thermodynamic integration that confirmed the existence of the monolayer over a small region. It will be interesting to study the phase behavior of different aspect ratio of the prolate and oblate particles to verify the existence of the monolayer with the presence of the nematic phase.

Supporting Information

Supporting Information is available from the Wiley Online Library or from the author.

Acknowledgements

The authors would like to acknowledge IIT Delhi HPC facility for computational resources. V.A.V. would like to acknowledge UGC-CSIR funding agency for the fellowship. S.B.B. acknowledges the partial support from DST-SERB India (Project No. CRG/2019/000580).

Conflict of Interest

The authors declare no conflict of interest.

Data Availability Statement

The data that support the findings of this study are available from the corresponding author upon reasonable request.

Keywords

material modeling, soft matter, self assembly

Received: September 12, 2022
Revised: December 7, 2022
Published online: January 11, 2023

[1] M. A. Boles, M. Engel, D. V. Talapin, *Chem. Rev.* **2016**, *116*, 11220.
[2] N. M. Silvestre, Q. Liu, B. Senyuk, I. I. Smalyukh, M. Tasinkevych, *Phys. Rev. Lett.* **2014**, *112*, 225501.
[3] A.-P. Hynninen, J. H. J. Thijssen, E. C. M. Vermolen, M. Dijkstra, A. van Blaaderen, *Nat. Mater.* **2007**, *6*, 202.
[4] D. Lyu, W. Xu, J. E. L. Payong, T. Zhang, Y. Wang, *Nat. Commun.* **2022**, *13*, 3980.
[5] M. Liu, X. Zheng, V. Grebe, M. He, D. J. Pine, M. Weck, *Angew. Chem., Int. Ed.* **2021**, *60*, 5744.
[6] M. He, J. P. Gales, t. Ducrot, Z. Gong, G.-R. Yi, S. Sacanna, D. J. Pine, *Nature* **2020**, *585*, 524.
[7] F. Smallenburg, F. Sciortino, *Nat. Phys.* **2013**, *9*, 554.
[8] Y. Liu, J. Wang, I. Imaz, D. Maspoch, *143*, 12943.
[9] H. Zargartalebi, S. H. Hejazi, A. Sanati-Nezhad, *Nat. Commun.* **2022**, *13*, 3085.
[10] C. Avci, Y. Liu, J. A. Pariente, A. Blanco, C. Lopez, I. Imaz, D. Maspoch, *Small* **2019**, *15*, 1902520.
[11] L. A. Galuska, E. S. Muckley, Z. Cao, D. F. Ehlenberg, Z. Qian, S. Zhang, S. Rondeau-Gagné, M. D. Phan, J. F. Ankner, I. N. Ivanov, X. Gu, *Nat. Commun.* **2021**, *12*, 2347.
[12] Y.-W. Sun, Z.-W. Li, Z.-Q. Chen, Y.-L. Zhu, Z.-Y. Sun, *Soft Matter* **2022**, *18*, 2654.
[13] Y.-J. Kim, J.-B. Moon, H. Hwang, Y. S. Kim, G.-R. Yi, *Adv. Mater.* **2022**, 2203045, https://doi.org/10.1002/adma.202203045.
[14] S. Mushnoori, J. A. Logan, A. V. Tkachenko, M. Dutt, *J. Chem. Phys.* **2021**, *156*, 024501.
[15] S. Corezzi, C. De Michele, E. Zaccarelli, D. Fioretto, F. Sciortino, *Soft Matter* **2008**, *4*, 1173.
[16] K. Gvozden, S. Novak Ratajczak, A. G. Orellana, E. Kentzinger, U. Rücker, J. K. G. Dhont, C. De Michele, E. Stiakakis, *Small* **2022**, *18*, 2104510.
[17] C. Karner, C. Dellago, E. Bianchi, *Soft Matter* **2020**, *16*, 2774.
[18] S. Wang, S. Lee, J. S. Du, B. E. Partridge, H. F. Cheng, W. Zhou, V. P. Dravid, B. Lee, S. C. Glotzer, C. A. Mirkin, *Nat. Mater.* **2022**, *21*, 580.
[19] E. Bianchi, J. Largo, P. Tartaglia, E. Zaccarelli, F. Sciortino, *Phys. Rev. Lett.* **2006**, *97*, 168301.
[20] F. Romano, F. Sciortino, *Soft Matter* **2011**, *7*, 5799.
[21] Z. Preisler, T. Vissers, F. Smallenburg, G. Munaó, F. Sciortino, *J. Phys. Chem. B* **2013**, *117*, 9540.
[22] L. Hong, A. Cacciuto, E. Luijten, S. Granick, *Nano Lett.* **2006**, *6*, 2510.
[23] Y. Wang, Y. Wang, D. R. Breed, V. N. Manoharan, L. Feng, A. D. Hollingsworth, M. Weck, D. J. Pine, *Nature* **2012**, *491*, 51.
[24] A. M. Jackson, J. W. Myerson, F. Stellacci, *Nat. Mater.* **2004**, *3*, 330.
[25] W. Li, J. D. Gunton, *Langmuir* **2013**, *29*, 8517.
[26] S. Sacanna, D. J. Pine, *Curr. Opin. Colloid Interface Sci.* **2011**, *16*, 96.
[27] G. Odriozola, *J. Chem. Phys.* **2012**, *136*, 134505.
[28] J. C. Gimel, D. Durand, T. Nicolai, *Phys. Rev. B* **1995**, *51*, 11348.
[29] J. C. Gimel, T. Nicolai, D. Durand, *J. Sol-Gel Sci. Technol.* **1999**, *15*, 129.
[30] S. Babu, J.-C. Gimel, T. Nicolai, C. De Michele, *J. Chem. Phys.* **2008**, *128*, 204504.
[31] A. Prabhu, S. B. Babu, J. S. Dolado, J.-C. Gimel, *J. Chem. Phys.* **2014**, *141*, 024904.
[32] V. A. Varma, I. Malhotra, S. B. Babu, *Phys. Rev. E* **2022**, *106*, 014602.
[33] S. Babu, J. C. Gimel, T. Nicolai, *J. Chem. Phys.* **2006**, *125*, 184512.
[34] S. Babu, J.-C. Gimel, T. Nicolai, *J. Chem. Phys.* **2009**, *130*, 064504.
[35] S. Babu, J. C. Gimel, T. Nicolai, *Eur. Phys. J. E* **2008**, *27*, 297.
[36] M. Rottereau, J. C. Gimel, T. Nicolai, D. Durand, *Eur. Phys. J. E* **2004**, *15*, 133.
[37] M. Rottereau, J. C. Gimel, T. Nicolai, D. Durand, *Eur. Phys. J. E* **2004**, *15*, 141.
[38] Z. Shireen, S. B. Babu, *J. Chem. Phys.* **2017**, *147*, 054904.
[39] Z. Shireen, S. B. Babu, *Soft Matter* **2018**, *14*, 9271.
[40] I. Malhotra, S. B. Babu, *Pure Appl. Chem.* **2018**, *90*, 1085.
[41] I. Malhotra, S. B. Babu, *J. Chem. Phys.* **2019**, *151*, 084901.
[42] I. Malhotra, S. B. Babu, *J. Phys.: Condensed Matter* **2020**, *32*, 355101.
[43] R. Martoňák, A. Laio, M. Parrinello, *Phys. Rev. Lett.* **2003**, *90*, 075503.
[44] L. Filion, M. Marechal, B. van Oorschot, D. Pelt, F. Smallenburg, M. Dijkstra, *Phys. Rev. Lett.* **2009**, *103*, 188302.
[45] D. Gottwald, G. Kahl, C. N. Likos, *J. Chem. Phys.* **2005**, *122*, 204503.
[46] E. Bianchi, G. Doppelbauer, L. Filion, M. Dijkstra, G. Kahl, *J. Chem. Phys.* **2012**, *136*, 214102.
[47] Z. Preisler, T. Vissers, F. Smallenburg, G. Munaó, F. Sciortino, *J. Phys. Chem. B* **2013**, *117*, 9540.
[48] T. Vissers, Z. Preisler, F. Smallenburg, M. Dijkstra, F. Sciortino, *J. Chem. Phys.* **2013**, *138*, 164505.
[49] Q. Chen, S. C. Bae, S. Granick, *Nature* **2011**, *469*, 381.
[50] D. Frenkel, A. J. C. Ladd, *J. Chem. Phys.* **1984**, *81*, 3188.
[51] C. Vega, E. Sanz, J. L. F. Abascal, E. G. Noya, *J. Phys. Condens. Matter.* **2008**, *20*, 153101.
[52] T. Vissers, Z. Preisler, F. Smallenburg, M. Dijkstra, F. Sciortino, *J. Chem. Phys.* **2013**, *138*, 164505.
[53] D. Frenkel, B. Smit, *Understanding Molecular Simulation*, Academic Press, Boston, MA **1996**.
[54] D. J. Kraft, R. Ni, F. Smallenburg, M. Hermes, K. Yoon, D. A. Weitz, A. van Blaaderen, J. Groenewold, M. Dijkstra, W. K. Kegel, *Proc. Natl. Acad. Sci. U. S. A.* **2012**, *109*, 10787.
[55] R. Pool, P. G. Bolhuis, *J. Phys. Chem. B* **2005**, *109*, 6650.
[56] R. Eppenga, D. Frenkel, *Mol. Phys.* **1984**, *52*, 1303.
[57] D. A. Kofke, *J. Chem. Phys.* **1993**, *98*, 4149.
[58] D. A. Kofke, *Mol. Phys.* **1993**, *78*, 1331.